Biogenic particles formed in the Himalaya as an important source of free tropospheric aerosols

Bianchi, F.

Bianchi , F , Junninen , H , Bigi , A , Sinclair , V A , Dada , L , Hoyle , C R , Zha , Q , Yao , L ,
Ahonen , L R , Bonasoni , P , Buenrostro Mazon , S , Hutterli , M , Laj , P , Lehtipalo , K ,
Kangasluoma , J , Kerminen , V -M , Kontkanen , J , Marinoni , A , Mirme , S , Molteni , U ,
Petäjä , T , Riva , M , Rose , C , Sellegri , K , Yan , C , Worsnop , D R , Kulmala , M ,
Baltensperger , U & Dommen , J 2021 , ' Biogenic particles formed in the Himalaya as an
important source of free tropospheric aerosols ' , Nature Geoscience , vol. 14 , no. 1 , pp.
4-+ . https://doi.org/10.1038/s41561-020-00661-5

acceptedVersion

Injections of newly formed biogenic particles in the Himalayan free troposphere

Authors. F. Bianchi[1], H. Junninen[1], A. Bigi[2], V. A. Sinclair[1], L. Dada[1], C.R. Hoyle[3], Q. Zha[1], L. Yao[1], L. R. Ahonen[1], P. Bonasoni[4], S. Buenrostro Mazon[1], M. Hutterli[5], P. Laj[1,4,6], K. Lehtipalo[1,7], J. Kangasluoma[1], V.-M., Kerminen[1], J. Kontkanen[1], A. Marinoni[4], S. Mirme[8], U. Molteni[3], T. Petäjä[1], M. Riva[1,a], C. Rose[1], K. Sellegri[9], C. Yan[1], D.R. Worsnop[10], M. Kulmala[1,11], U. Baltensperger[3], J. Dommen[3]

Addresses.

[1]Institute for Atmospheric and Earth System Research / Physics, University of Helsinki, 00014 Helsinki, Finland

[2]Department of Engineering 'Enzo Ferrari', University of Modena and Reggio Emilia, 41124 Modena, Italy

[3]Laboratory of Atmospheric Chemistry, Paul Scherrer Institute, 5232 Villigen, Switzerland

[4]CNR-ISAC, National Research Council of Italy – Institute of Atmospheric Sciences and Climate, Bologna, Italy

[5]TOFWERK AG, 3600 Thun, Switzerland

[6]Univ. Grenoble Alpes, CNRS, IRD, Grenoble INP, Institute for Geosciences and Environmental Research (IGE), 38000 Grenoble, France

[7]Finnish Meteorological Institute, 00560 Helsinki, Finland

[8]Institute of Physics, University of Tartu, 50090 Tartu, Estonia

[9]Laboratoire de Météorologie Physique (LaMP), CNRS UMR 6016, Université Blaise Pascal, Aubière, 60026, France

[10]Aerodyne Research, Billerica, MA 01821, USA.

[11]Aerosol and Haze Laboratory, Beijing Advanced Innovation Center for Soft Matter Science and Engineering, Beijing University of Chemical Technology, 100029 Beijing, P.R. China

[a]now at: the Univ Lyon, Université Claude Bernard Lyon 1, CNRS, IRCELYON, 69626, Villeurbanne, France

Corresponding author: federico.bianchi@helsinki.fi

Aerosols of biogenic and anthropogenic origin affect the total radiative forcing of global climate. Poor knowledge of the pre-industrial aerosol concentration and composition, in particular of particles formed directly in the atmosphere from gaseous precursors, constitutes a large uncertainty in the anthropogenic radiative forcing. Investigations of new particle formation at preindustrial-like conditions can contribute to the reduction of this uncertainty. Here we present observations taken at the remote Nepal Climate Observatory Pyramid station at 5079 m a.s.l., a few km from the summit of Everest. We show that up-valley winds funnel gaseous aerosol precursors to higher altitudes. During this transport, these are oxidised to compounds of very low volatility, which rapidly form a large number of aerosol particles. These are then transported into the free troposphere, suggesting that the whole Himalayan region may act as an "aerosol factory", contributing substantially to the free tropospheric aerosol population. Aerosol production in this region occurs mainly via organic precursors of biogenic origin with little evidence of the involvement of anthropogenic pollutants. This process is therefore likely to be essentially unchanged since the pre-industrial period, and may have been one of the major sources contributing to the upper tropospheric aerosol population during that time.

Atmospheric aerosols are extensively studied as they can interact directly with solar radiation, or indirectly by modifying cloud properties. Accordingly, aerosols affect the global climate, yet the resulting total radiative forcing is still highly uncertain[1]. New particle formation (NPF), through transformation of gaseous precursors, contributes a major fraction to the total global cloud condensation nuclei budget[2–4]. Many laboratory experiments and measurements in the boundary layer have been conducted to elucidate this phenomenon. Among those, in two notable studies[5,6] nucleation of pure organic species in the absence of sulfuric acid was observed in the CLOUD chamber. A recent atmospheric study confirmed that organics can indeed play a major role in NPF at high altitudes in the Alps[7]. However, this has been the only study so far that gave insight into the chemical composition of newly formed particles at high altitude.

New particle formation on top of the Himalaya. A pioneering study investigated NPF at the Nepal Climate Observatory - Pyramid (NCO-P, Supplementary Fig. 1), located at 5079 m a.s.l. near the base camp of Mt. Everest, where a quasi-daily occurrence of NPF events was observed[8,9]. However, the lack of instrumentation for chemical speciation left the identity of the species involved in NPF unresolved, and no quantification of the particle flux could be given. Here, we deployed a set of instruments at NCO-P to measure the size distribution of particles (diameter $d >$ 1nm) and ions ($d >$ 0.8 nm) as well as the chemical composition of the cluster ions. This included a particle size magnifier (PSM), a Neutral cluster and Air Ion Spectrometer (NAIS), and an atmospheric pressure interface time-of-flight (APi-TOF) mass spectrometer. In addition, a nitrate based chemical ionisation unit permitted the measurement of the neutral compounds (CI-APi-TOF). These instruments were complemented by the long-term instrumentation running at NCO-P such as a scanning mobility particle sizer (SMPS), and ozone and SO_2 monitors.

Observations were conducted during the post-monsoon period (28 November 2014 – 25 December 2014), when clean conditions prevail, with little transportation from the Indo-Gangetic plain, and NPF is frequent[9–11]. In agreement with previous studies, we encountered a very high frequency of

NPF events (Extended Data Fig. 1) where both nanoparticles and cluster ions grew rapidly to sizes larger than 10 nm (Fig. 1a and Extended Data Fig. 1). While Extended Data Fig. 1 shows all the events individually, Fig. 1a shows the average of all events to demonstrate the high degree of consistency among these events. Since the events start at slightly different times, the typical banana shape is slightly blurred, yet clearly seen in Extended Data Fig. 1. The appearance of clusters and nanoparticles associated with NPF started between 08:30 and 12:30 local time (Supplementary Table 1), whereas the particle growth to larger sizes continued until the late afternoon. The mean number size distribution binned by wind direction (Fig. 1b) clearly shows that the great majority of the growing nanoparticles were related to south-westerly wind conditions, i.e. up-valley wind (195°-205°). The average size distribution of the particles measured at NCO-P, including all campaign days, illustrates the predominance of NPF events (Fig. 1a), even though the variability of both the NPF starting times, and the location at which NPF is initiated with respect to NCO-P, hides the characteristic NPF shape seen in the individual events (Extended Data Fig. 1).

The circulation of the air masses at NCO-P was examined with wind data from four sites along the Khumbu valley between Lukla (2660 m a.s.l.) and NCO-P (5079 m a.s.l.) (available from 2002 to 2012, Supplementary Fig. 4). The average wind roses over November – December show that the up-valley wind starts at all sites around 09:00 simultaneously (i.e. at all sites within 1 hour, given the resolution of the wind data) and it lasts until about 17:00, when the down-valley wind starts (Extended Data Fig. 2 and Supplementary Figs. 5, 6 and 7).

The initiation of NPF at NCO-P was characterized by a steep increase in the concentration of particles with 1.1-2.1 nm diameter and ions (Fig. 2 and Extended Data Fig. 3). A corresponding increase in concentration was observed for particles measured by the NAIS (3.2 to 42 nm; red in Fig. 2a) and the SMPS ($d > 43$ nm, light blue in Fig. 2a). For both the positive (Fig. 2b) and negative (Extended Data Fig. 3a) ions detected by the APi-TOF, the concentrations in the largest size bin (with mass to charge ratios m/z in the range $500 < m/z < 1000$) increased during the nucleation

event, while the concentrations of medium ($250 < m/z < 500$) and small ($m/z < 250$) ions stayed constant and decreased, respectively, indicating the formation of larger ion clusters during NPF. While Fig. 2 results from an averaging of more than 20 NPF events, Extended Data Fig. 3b shows the temporal evolution for just one day during a new particle formation event (06 December). Exactly when the wind direction changes and the valley wind starts, NPF is triggered as seen in the changes in the mass spectrometer signals and in the smallest channel of the NAIS, while the increase in the other channels of the NAIS occurs at a later time. From this we determined median growth rates of 2.7, 5.7 and 10 nm/h for the particle size ranges of <3, 3-7 and 7-30 nm, respectively (Extended Data Fig. 4). Thus, for particles to grow to 2 nm new paticle formation must happen within 10 km down the valley at a wind speed of 2-3 m/s (Supplementary Fig. 9).

Chemical composition of gaseous molecules and clusters. Figure 3 shows the chemical composition of the positive and negative ions (Panel a and b) for two individual days, and Fig. 4 shows their time evolution (Panel a and b) during NPF. In both configurations (positive and negative ions), we observed a large fraction of organic compounds (green) with a chemical composition of $C_xH_yO_z$ and a high O:C ratio, indicating the formation of highly oxygenated organic molecules[12] (HOMs). As seen in Figs. 2b, 4 and Supplementary Fig. 2, a higher abundance of larger ions was found during the event than before the event. This increase in the abundance of high molecular weight signals was observed in positive, negative, and neutral mode, but was most evident for the positive ions where compounds or molecular clusters containing up to 10, 15 or even 20 carbon atoms were found. During the events, even larger ions were present, which, although not unambiguously identified, were most likely organic, with a correspondingly higher number of carbon atoms. Similarly to APi-TOF observations at another mountainous location[7] and in the boreal forest[13,16], the three main negative ion peaks during sunny days are HSO_4^-, $H_2SO_4HSO_4^-$ and $(H_2SO_4)_2HSO_4^-$. However, based on laboratory[17,18] and field observations[7], the absence of sulfur containing peaks at higher masses rules out pure sulfuric acid or sulfuric acid – base nucleation.

This is confirmed in Fig. 4b where the estimated level of a sulfuric acid proxy (red dots) and the sulfuric acid ion clusters (orange line) rise at the same time following the solar radiation, 1 to 2 hours before the beginning of NPF. In contrast, most other peaks (mainly organics) rise at the same time as NPF starts. This rise correlates with the wind but not with the radiation, highlighting once more the importance of the transport of organic vapours to the site.

The results given so far indicate consistently that the observed NPF events must be due to nucleation of HOMs. In the positive ion mass spectra we see a series of strong peaks appearing above m/z 200, which could be identified as $C_{10}H_{16,18}O_x$ and $C_{15}H_{24}O_x$ compounds clustered to NH_4^+ or $(NH_3)NH_4^+$ (Supplementary Table 2). While $C_{10}H_{16,18}O_x$ are most likely oxidation products from terpenes, the $C_{15}H_{24}O_x$ compounds can be assigned either to oxidation products of sesquiterpenes, clusters of terpene and isoprene HOMs, or clusters of terpene HOMs with C5-amines. Despite of this difficulty in peak assignment, it strongly indicates that these ions are oxidation products of biogenic precursors.

The emissions of volatile organic compounds (VOCs) in the Khumbu Valley have not been accurately inventoried so far. In the Himalaya[19], mixed vegetation, including grass and needle leaf forest/shrub, is present up to 5000 m (forest < 4000 m) and likely emits a wide variety of biogenic VOCs such as isoprene, monoterpenes and sesquiterpenes[20]. From laboratory experiments[5,6], it is known that oxidation products of monoterpenes can trigger NPF on their own. During all NPF events the wind speed was sufficient to transport an air mass from vegetated areas to NCO-P in a short time period (typically less than an hour). While the nucleation mode (d < 20 nm) particle number concentration rapidly increased after the onset of southerly winds and peaked 2 hours later (Fig. 2 and Extended Data Fig. 5), the concentrations of equivalent black carbon (eBC) and particulate matter with an aerodynamic diameter smaller than 1 μm (PM_1) started to rise only slowly and reached a maximum when the southerly winds ceased around 6 to 7 hours later. The distinctly different temporal evolution of the nucleation mode particles compared to eBC, a tracer of

anthropogenic pollution, and PM_1 indicates a weak influence of anthropogenic pollutants on NPF. Furthermore, the maximum concentration of eBC and PM_1 in the late afternoon is roughly a factor 2-3 lower than reported in long-term studies for the post-monsoon period[9,11]. In addition, as outlined in the Supplementary Information, the concentration of aromatic precursors at NCO-P is estimated to be more than an order of magnitude smaller than would be required for NPF to occur. Thus, there is strong evidence that NPF during this period was caused by biogenic compounds emitted in the Khumbu valley and transformed to HOMs by ozonolysis and OH radical reactions.

Simulation of the transport of newly formed particles. To determine where the newly formed particles are subsequently transported to, we performed forward particle trajectory calculations for 5 different days (17 – 21 December 2014). The four days of 18-21 December were NPF days representative of the overall campaign while the day of 17 December was included as an example of a sunny day when no NPF was observed.

Using the Weather Research and Forecasting (WRF)[21] model we generated a gridded data set of meteorological variables at a horizontal resolution of 1 km. There is good agreement between the model and observations at NCO-P for wind direction and speed (Extended Data Fig. 6 and Supplementary Figs. 9 and 10). We then used the WRF model output as input to the Lagrangian Particle dispersion model FLEXPART-WRF[22]. For each day between 17 and 21 December 2014 a total of 2 million passive tracers were released at a height of 0 – 10 meters above ground level at NCO-P. The particles were released at a constant rate between 08:45 and 14:45 local time every day, including 17 December when no NPF was observed.

The FLEXPART-WRF (hereafter FLEXPART) results show that for all 5 days the passive tracers are rapidly transported vertically away from the surface (Supplementary Fig. 11) and then travel horizontal distances of hundreds of kilometres in a few hours (Fig. 5a, Extended Data Fig. 7 and Supplementary Figs. 12 – 15). On 21 December, with high wind speeds (~20 km h^{-1} at the station), the mean position of the particles was ~32 km (~65 km) to the north after 1 hour (2 hours). The

height above sea level of the mean trajectories is very similar on the 4 days when NPF was observed, typically 5 to 6 km, while on 17 December, the mean trajectory height is much lower (Fig. 5a and Supplementary Fig. 11a). On the NPF days the local valley winds lifted the particles to altitudes where synoptic-scale winds are strong. Once transported upwards, these particles are far above the boundary layer and they stay at this altitude also when leaving the mountainous area. The mean height of the passive tracers above local ground level is 1 km after just 6 hours for all five days and on 20 December exceeds 2.4 km after 12 hours, more than a hundred kilometres downwind of the Pyramid station (Supplementary Fig. 11b). Away from the mountainous area, the mean mixed layer depth calculated by FLEXPART is typically 1 km during daytime but only a few hundred meters at night and early morning (Supplementary Fig. 16). Therefore, although estimates of the mixed layer depth over complex terrain from numerical models must be treated with caution (reference 23 and references therein), the FLEXPART simulations indicate that after 6 hours, 70 - 80% of the passive tracers are transported out of the mixed layer (Extended Data Fig. 8). Similar mountain venting has been noted previously[24] and confirmed by airborne lidar measurements.[25]

Implication for aerosol concentration in the free troposphere. Assuming a boundary layer depth of 300 m on NPF event days at NCO-P we estimate that about $2.1 \cdot 10^{20}$ ($6.5 \cdot 10^{19} - 1.3 \cdot 10^{21}$) particles with $10 < d < 50$ nm were transported by the valley wind out of the valley during each NPF day (Fig. 5c). These particles are injected into the upper tropospheric air mass and rapidly transported away and diluted (Fig. 5a). After 9-12 hours these particles are distributed into a volume of 3000-30000 km^3 resulting in an average concentration of 10-100 cm^{-3} as simulated by the FLEXPART model (Fig. 5b). The Duth Koshi basin has about 3-5 valleys similar to the one with the NCO-P station within 40 km, which most probably act as similar sources of particles into the upper troposphere. If this number of valleys is considered representative of the southern slope of the Himalaya (Supplementary Fig. 17), a particle plume from one valley will take up along its trajectory of 80 to 150 km vented particles from 4-12 similar valleys. This may increase the particle concentration by

up to several 100 cm^{-3}. In this study the concentration of particles $10<d<42$ nm before nucleation started was around 450 cm^{-3} (median) while Reference 9 reported 50-100 cm^{-3} for particles $10<d<20$ nm on non-event days over a period of one year.

We conclude that a coupled atmospheric chemistry-dynamics mechanism efficiently forms and transports particles to high altitude, where they are transported further over long distances. Thus, the Himalayas act as a "free tropospheric aerosol factory" increasing the background aerosol concentration by a factor up to 2 or more. This mechanism is driven by the oxidation of organic compounds transported by an up-valley wind system. Since the origin of the precursor is most probably biogenic, and sulfuric acid is not significantly involved in the NPF process, it is likely that this large and frequent source of free tropospheric aerosol was also present in the pre-industrial time, when other mechanisms of free tropospheric NPF were less efficient than today, due to lower SO$_2$ concentrations[3]. If the organic precursor were of anthropogenic origin, then this pure organic nucleation mechanism would still constitute another important way of particle transport into the free troposphere influencing present day cloud formation in the Himalayas and northern India region. Permanent measurements, and new instruments with higher mass spectral resolution, will allow to discriminate between these two possibilities.
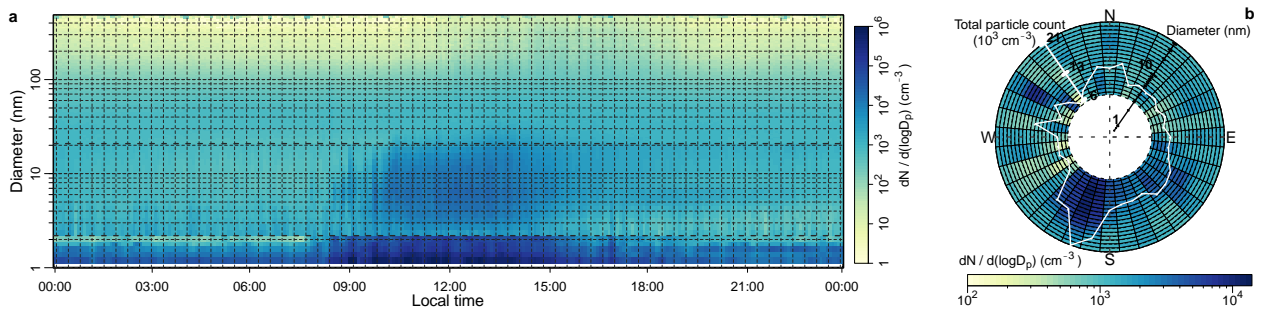
FIGURES

Figure 1. Size distribution of aerosol particles observed at the NCO-P station. a, Average particle number size distribution (from 1.1 nm to 488 nm) during the whole campaign (PSM: $1.1 < d < 2.1$ nm; NAIS: $3.2 < d < 21$ nm; SMPS: $d > 21$nm). **b**, Campaign average particle number size distribution (2.5 – 42 nm) binned by wind direction (30 min integration time). The white line shows the average particle concentration.
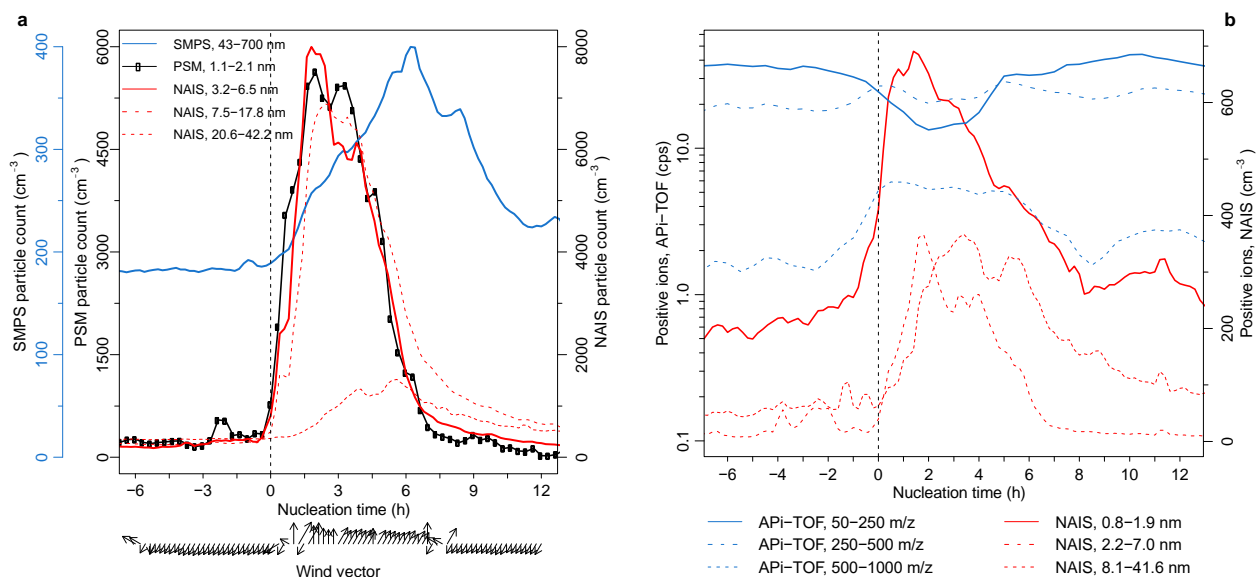
Figure 2. Influence of wind direction on the diurnal variation of ion cluster and particle concentrations. a, Mean patterns for the total particle number concentrations at different sizes during all the NPF events ($1.2 < d < 2.1$ nm measured by the PSM (black), $3.2 < d < 42.2$ nm measured by the NAIS (red) and larger particles ($d > 43$ nm) measured by the SMPS (blue). The mean pattern for the wind vector is also shown. **b**, Mean patterns for positive ions from the NAIS as well as for selected *m/z* ranges measured by the APi-TOF during all the NPF events when the APi-TOF was measuring in positive mode (see Supplementary Table 1). Aerosol and ion data in a and b were aggregated by defining the first enhanced 12-min value of the NPF event as time zero. The start of each NPF event was detected by inspecting the time series of the total number concentration of negative ions with $1.5 < d < 2$ nm measured by the NAIS.
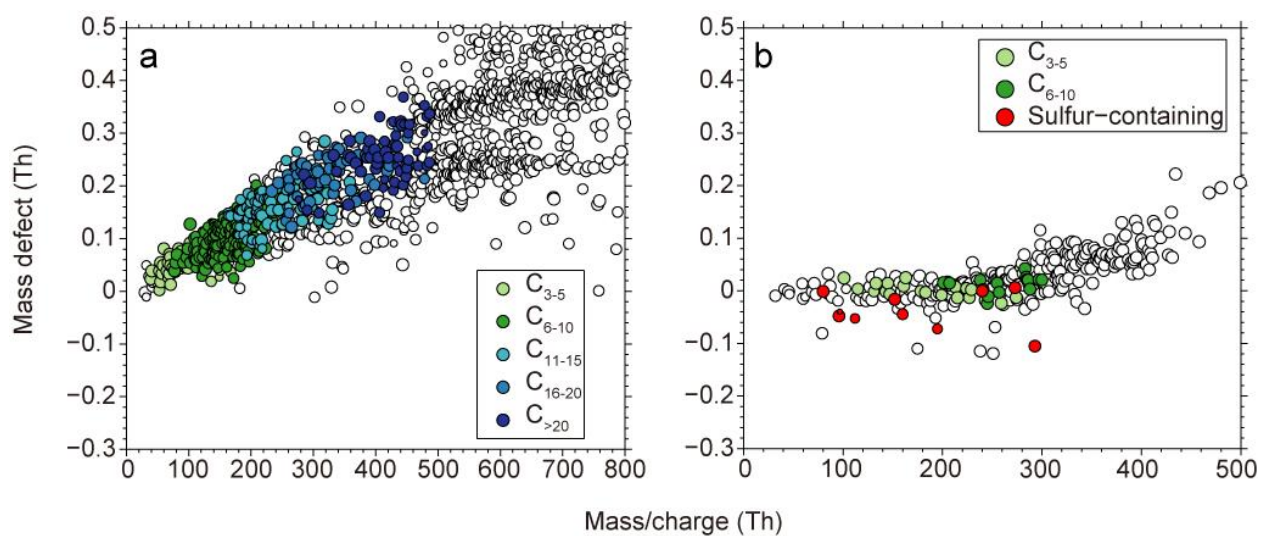
Figure 3. Chemical composition of the positive and negative ions (molecules and clusters) during NPF events. a, Mass defect (MD) plot of positive ions averaged from 12:00 – 15:00 on 09 December 2014; **b**, MD plot of negative ions averaged from 12:00 – 15:00 on 22 December 2014. The size of the circles is proportional to the intensity of the signal.
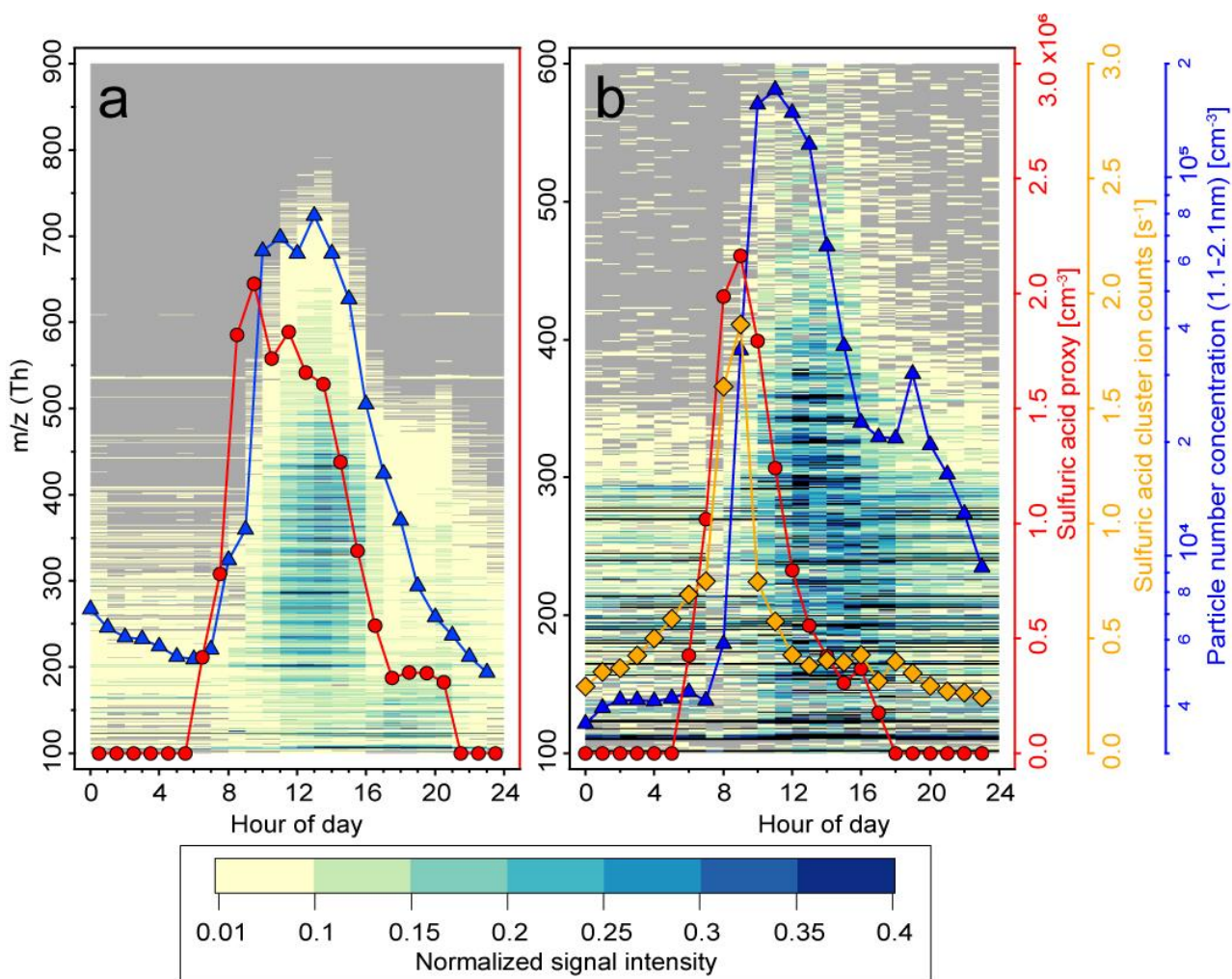
Figure 4. Diurnal evolution of positive and negative ions, a sulfuric acid proxy and concentration of recently formed particles. a, Hourly averaged time evolution of the positive ion mass spectra from 07 to 10 December 2014. **b**, Hourly averaged time evolution of the negative ions mass spectra from 21 to 25 December 2014. The red line in panel a and b represents the sulfuric acid proxy and the orange line shows the sulfuric acid ion clusters signal. Finally the blue line shows the very small particles between 1 and 2.1 nm. Particle number concentrations correlate very well with the appearance of organics at high *m/z* in the APiTOF while sulfuric acid ions correlate with the sulfuric acid proxy and are not related to the NPF events, both confirming that organics drive NPF and not sulfuric acid.
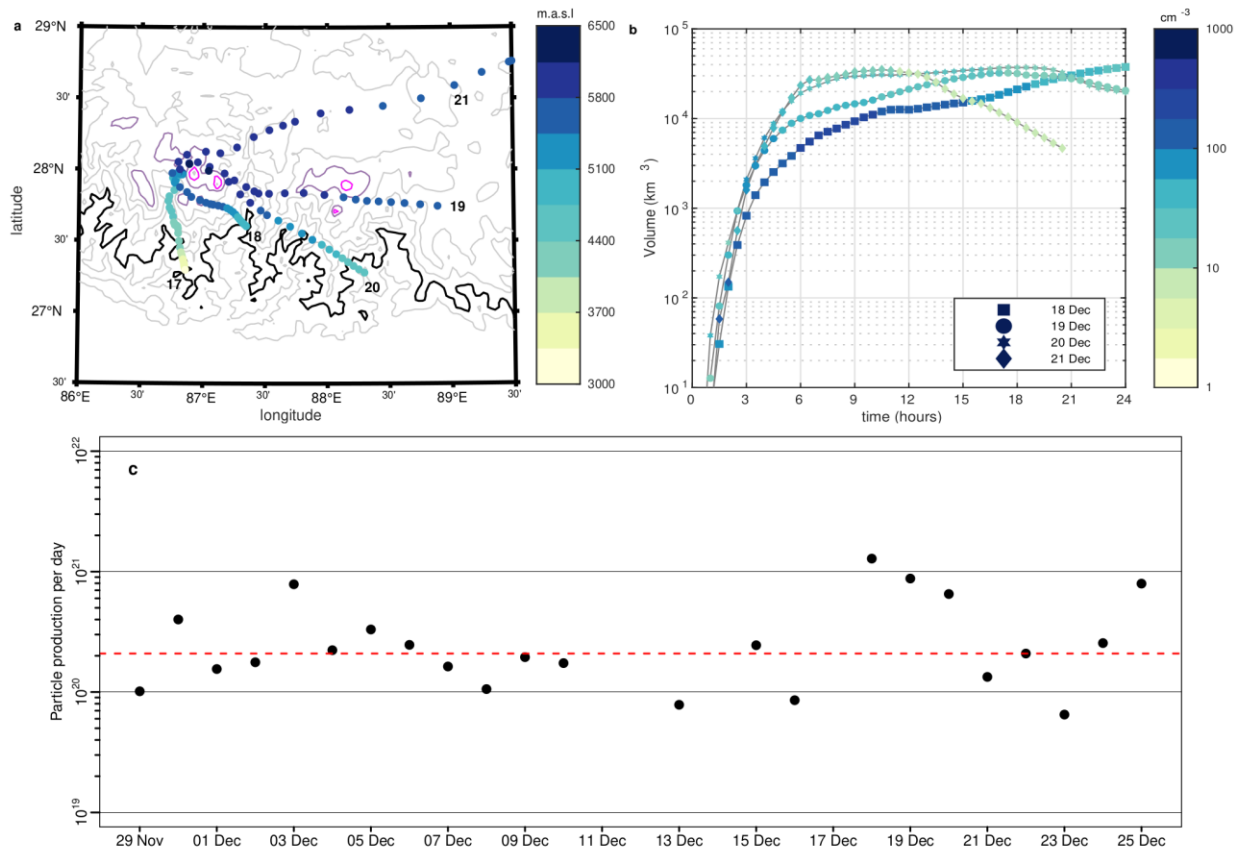
Figure 5. FLEXPART-WRF simulation of the transport of passive tracers released at the Pyramid station. Height, position and concentrations of passive tracers are simulated by FLEXPART-WRF (forward trajectories starting from the Pyramid station) for 5 different days (17-21 December 2014). The mean locations of the passive tracers are shown in **a** every 30 minutes where colours show the mean height of the tracers above sea level. Topography is shown as contours (black: 2 km a.s.l., purple: 6 km a.s.l., magenta: 7 km a.s.l.). Light gray contours show topography every 1 km. **b**, Simulated average concentration of particles for a volume wherein the particle concentration is > 1 cm^{-3} in each grid point. **c**, Daily production of particles in the size range between 10 and 50 nm formed until the end of the Khumbu valley, which are then vented out of the valley. The red dashed line presents the median of $2.1 \cdot 10^{20}$ particles per day.

References

1. IPCC *Climate change 2013: the physical science basis. contribution of Working Group I to the fifth assessment report of the Intergovernmental Panel on Climate Change*. 1535 (Cambridge University Press: Cambridge, United Kingdom and New York, NY, USA, 2013)

2. Dunne, E. M. *et al.* Global atmospheric particle formation from CERN CLOUD measurements. *Science* **354**, 1119–1124 (2016).

3. Gordon, H. *et al.* Causes and importance of new particle formation in the present-day and preindustrial atmospheres. *J. Geophys. Res. Atmos.* **122**, 8739–8760 (2017).

4. Merikanto, J., Spracklen, D. V., Mann, G. W., Pickering, S. J. & Carslaw, K. S. Impact of nucleation on global CCN. *Atmos. Chem. Phys.* **9**, 8601–8616 (2009).

5. Kirkby, J. *et al.* Ion-induced nucleation of pure biogenic particles. *Nature* **533**, 521–526 (2016).

6. Tröstl, J. *et al.* The role of low-volatility organic compounds in initial particle growth in the atmosphere. *Nature* **533**, 527–531 (2016).

7. Bianchi, F. *et al.* New particle formation in the free troposphere: A question of chemistry and timing. *Science* **352**, 1109–1112 (2016).

8. Sellegri, K. *et al.* Seasonal variations of aerosol size distributions based on long-term measurements at the high altitude Himalayan site of Nepal Climate Observatory-Pyramid (5079 m), Nepal. *Atmos. Chem. Phys.* **10**, 10679–10690 (2010).

9. Venzac, H. *et al.* High frequency new particle formation in the Himalayas. *Proc. Natl Acad. Sci.* **105**, 15666–15671 (2008).

10. Bonasoni, P. *et al.* Atmospheric brown clouds in the himalayas: first two years of continuous observations at the Nepal Climate Observatory-Pyramid (5079 m). *Atmos. Chem. Phys.* **10**, 7515–7531 (2010).

11. Marinoni, A. *et al.* Aerosol mass and black carbon concentrations, a two year record at NCO-P (5079 m, Southern Himalayas). *Atmos. Chem. Phys.* **10**, 8551–8562 (2010).

12. Bianchi, F. *et al.* Highly Oxygenated Organic Molecules (HOM) from Gas-Phase Autoxidation Involving Peroxy Radicals: A Key Contributor to Atmospheric Aerosol. *Chem. Rev.* **119**, 3472–3509 (2019).

13. Bianchi, F. *et al.* The role of highly oxygenated molecules (HOMs) in determining the composition of ambient ions in the boreal forest. *Atmos. Chem. Phys.* **17**, 13819–13831 (2017).

14. Eisele, F. L. & Tanner, D. J. Measurement of the gas phase concentration of H2SO4 and methane sulfonic acid and estimates of H2SO4 production and loss in the atmosphere. *J. Geophys. Res. Atmos.* **98**, 9001–9010 (1993).

15. Kurtén, T. *et al.* The effect of H2SO4–amine clustering on chemical ionization mass spectrometry (CIMS) measurements of gas-phase sulfuric acid. *Atmos. Chem. Phys.* **11**, 3007–3019 (2011).

16. Ehn, M. *et al.* Composition and temporal behavior of ambient ions in the boreal forest. *Atmos. Chem. Phys.* **10**, 8513–8530 (2010).

17. Almeida, J. *et al.* Molecular understanding of sulphuric acid-amine particle nucleation in the atmosphere. *Nature* **502**, 359–363 (2013).

18. Kirkby, J. *et al.* Role of sulphuric acid, ammonia and galactic cosmic rays in atmospheric aerosol nucleation. *Nature* **476**, 429–433 (2011).

19. Bajracharya, B., Uddin, K., Chettri, N., Shrestha, B. & Siddiqui, S. A. Understanding land cover change using a harmonized classification system in the Himalaya. *Mt. Res. Dev.* **30**, 143–156 (2010).

20. Guenther, A. *et al.* A global model of natural volatile organic compound emissions. *J. Geophys. Res. Atmos.* **100**, 8873–8892 (1995).

21. Skamarock, W. C. *et al. A Description of the Advanced Research WRF version 3*. (National Center for Atmospheric Research: Boulder, Colorado, USA, 2008).

22. Brioude, J. *et al.* The Lagrangian particle dispersion model FLEXPART-WRF version 3.1. *Geosci. Model Dev*. **6**, 1889–1904 (2013).

23. De Wekker, S. F. J. & Kossmann, M. Convective boundary layer heights over mountainous terrain—a review of concepts. *Front. Earth Sci.* **3**, 77 (2015).

24. Henne, S. *et al.* Quantification of topographic venting of boundary layer air to the free troposphere. *Atmos. Chem. Phys.* **4**, 497–509 (2004).

25. Nyeki, S. *et al.* Airborne Lidar and in‑situ Aerosol Observations of an Elevated Layer, Leeward of the European Alps and Apennines. *Geophys. Res. Lett.* **29**, (2002).

CORRESPONDING AUTHOR: Correspondence and requests for materials should be addressed to Federico Bianchi (Federico.bianchi@helsinki.fi).

Author contributions

F.B. conceived the study and led the overall scientific questions. F.B. and H.J. organized and conducted the Himalayan expeditions. F.B., H.J., A.B., L.D., Q.Z., L.Y., K.L., J.Kon., A.M., U.M., M.R., C.R. and C.Y. made the data analysis. V.A.S. performed and analysed the WRF and FELXPART simulations. F.B., V.A.S., A.B., C.R.H., Q.Z., P.L., K.L., V.M.K., T.P., K.S., D.R.W., M.K., U.B. and J.D. made the data interpretation. L.R.A., P.B. M.H., J.Kan., S.B.M., S.M., A.M., U.M., have helped with logistic challenges, with instrument support and data quality assurance. P.B., P.L., A.M. and K.S. provided the measurement data from the long term observation. F.B., V.A.S., V.M.K., U.B. and J.D., wrote the manuscript with contributions from all authors.

Competing interests

The authors declare no competing interests.

METHODS

The Nepal Climate Observatory-Pyramid (NCO-P, 27.95 N, 86.82 E, Supplementary Fig. 1) is located at 5079 m a.s.l. in the Sagarmatha National Park near Mt. Everest in the eastern Nepal Himalaya. The Observatory stands at the top of a hill, at the confluence of the secondary Lobuche valley (oriented NNW-SSE) and the main Khumbu valley (oriented NE-SW), a tributary of the Duth Koshi valley, a major Ganges tributary.

The monitoring activity in the observatory is completely powered by energy from 112 photovoltaic panels, minimizing the possible influence of local emissions and guaranteeing air mass sampling under clean conditions. Quality control for instrumentation and data reduction are performed according to ACTRIS/GAW/AGAGE procedures for aerosols and gases.

Below 4 km a.s.l. the valley is covered by forests while the landscape around the measurement site is mostly rocky with patches of musk. The area is located away from important anthropogenic sources of pollutants, and only small villages are present along the valley (Namche Bazar, the biggest village of the valley, located at 3600 m a.s.l and 20 km from NCO-P, accounts for about 800 inhabitants). The closest major urban area is Kathmandu, located about 150 km south-west of the measurement site and 3.8 km lower in altitude, which is characterised by high atmospheric pollution and poor air quality.

At NCO-P the wind regime is characterised by a mountain/valley breeze circulation[9,10]. The valley winds start on average around 09:00 local time (LT), with maximum strength in the early afternoon, while during night-time, the wind flow reverses and shows lower intensity compared to the day-time valley winds (Extended Data Fig. 2). The NCO-P is clearly under free tropospheric conditions during the night while during the day the valley breeze transports trace gases from the lower part of the valley to the station.

In order to study new particle formation (NPF) events at NCO-P under conditions of low anthropogenic perturbation, we arranged our experiment during the post-monsoon season, which is the cleanest dry season with the least influence from regional/continental emissions[8,9,11,26].

At NCO-P, a wide range of measurements for aerosols and trace gases have been performed continuously since March 2006. These include:

- Surface ozone by a photometric O_3 analyser (Thermo Electron Corporation) operating at 254 nm. The sampling methodology was based on the GAW-WMO requirements[27].

- Aerosol light absorption coefficient measured by a multi-angle absorption photometer (MAAP 5012, Thermo Electron Corporation) operating at a wavelength of 637 nm, from which the equivalent black carbon (eBC) concentration is retrieved using a mass absorption cross section of 6.6 m^2 g^{-1}.

- Aerosol size distribution for particle diameters from 10 to 500 nm with a scanning mobility particle sizer (SMPS).

- Downward solar irradiance throughout the 305–2800 nm spectral range with a Kipp&Zonen CMP21 pyranometer.

- Wind speed and direction, atmospheric pressure, air temperature and relative humidity, precipitations with a VAISALA Weather Transmitter WXT510.

Additional instrumentation during this campaign.

Particle size magnifier (PSM)

The Airmodus A10 PSM[28] determines the size distribution of particles between 1 and 3 nm diameter. Particles grow inside the PSM with diethylene glycol (DEG) as a working fluid to about 90 nm in diameter, after which counting is performed with an Airmodus A20 butanol condensation particle counter (CPC). The cut-off size of the PSM can be varied by altering the mixing ratio of the

sample and DEG saturated flows. In this study, we used a 120-step scanning cycle between saturator flow rates of 0.1 and 1 l min^{-1}. Particle size calibrations were performed using ammonium sulfate particles produced in a tube furnace. These were size-classified with a high-resolution differential mobility analyser[29], and a supersaturation scan with the PSM was conducted for each selected size to obtain the relation between particle size and saturator flow rate. The data inversion was then performed by assuming Gaussian-shaped kernel functions yielding the particle concentration in five size bins between 1.1 and 2.1 nm[30]. These size classified concentrations were summed up in Fig. 2a to obtain the total concentration of particles between 1.1 and 2.1 nm. The PSM has been already used at high altitude in the Alps[7,31].

Neutral cluster and air ion spectrometer (NAIS)

Aerosols and ions were detected by a neutral cluster and air ion spectrometer by Airel Ltd. (NAIS). The NAIS is an ion mobility spectrometer which measures the number size distribution of ions and total (charged and neutral) particles with electrical mobilities ranging from 3.2 to 0.0013 cm^{2}V^{-1}s^{-1}, or 0.8 - 42 nm mobility diameter for ions and 2 - 42 nm for neutral particles[32,33]. Two DMAs classify the positive and negative ions. Each DMA has 21 electrometers, detecting charged particles of different mobilities. The high sample flow rate (54 l min^{-1}) allows the measurement of concentrations even below 100 cm^{-3}. The instrument switches periodically between different modes (ion, particle, offset), with one cycle typically lasting 150 s. In the ion mode, only ions and naturally charged particles are detected. In the particle mode, particles are charged using a corona charger before entering the DMA. At the end of each cycle the instrument switches to offset mode, i.e. removes all particles from the sample flow to determine the noise level.

On 3 December, 2014, the sample flow rate, was raised from the standard flow rate of 54 l min^{-1} to 75 l min^{-1}. The increase in concentration due to a higher flow rate was corrected during data processing by multiplying the number concentration by the ratio 54/75 (see Eq. 6 in reference 32).

We applied the small ion correction following reference 34, using their Table 2 where a= 0.713, b= 0.120 for inversion method "inv5"). Size-dependent transmission losses due to the inlet tube (tube length 80 cm and 3.3 cm width, temperature 0°C, pressure= 550 hPa) were corrected as well. The NAIS automatically increased its sheath-flow to 108 l min^{-1} to compensate for the effect of high altitude (lower atmospheric pressure) on particle mobility.

APi-TOF, CI-APi-TOF and cluster chemical composition

The chemical composition of the naturally charged ions were measured with the atmospheric pressure interface time of flight (APi-TOF, reference 35) mass spectrometer (Tofwerk AG, Thun, Switzerland & Aerodyne Research, Billerica, USA). In the APi section, the sample air passes through a critical orifice with a flow rate of 0.8 l min^{-1}, after which the ions are guided by two quadrupoles and an ion lens to the time-of-flight mass spectrometer. In this interface, the pressure is reduced from atmospheric level to 10^{-6} mbar inside the mass spectrometer. The mass spectrometer was operated in V mode (using one reflectron within the flight path of the ions), which favours sensitivity over resolution in the data acquisition. The mass accuracy was better than 5 ppm and the resolving power was around 5000 Th/Th. The instrument was also equipped with a chemical ionization unit (CI-APi-TOF) using nitric acid as the ionization reagent[36], enabling the determination of the chemical composition of the neutral compounds. Out of one month of data, we collected at least 7 days of either positive, negative or neutral clusters.

Unfortunately, the mass spectrometer suffered from some severe damage due to the lack of careful handling during transportation. After days of troubleshooting we succeeded in having an acceptable signal, although in the negative mode the transmission at high masses was very low. Therefore, we could not determine the chemical composition of negative ions and neutral clusters with *m/z* > 500 Th.

As seen in Supplementary Fig. 2 the *m/z* signal for the negative ions ranges only up to 500 Th, while it extends for the positive ions up to 900 Th. In both cases a decrease in the ion transmission above 400 Th is clearly visible. Thus, we were still able to determine the chemical composition of the clusters and to obtain information on the main compounds during nucleation. However, we were unfortunately unable to determine any concentrations when measuring the neutral compounds using the chemical ionisation unit with NO_3^- as primary ion.

Model Simulations

WRF Simulations

The Weather Research and Forecasting (WRF) model is a state-of-the-art numerical weather prediction model that can be applied to meteorological situations across a range of spatial and temporal scales. We use WRF version 3.6.1 and utilise the capability to run nested domains, where the nest is a finer resolution model run embedded within, and runs simultaneously with the coarser model domains.

Our simulation consists of a large (3618 km by 2997 km) outer domain with a grid spacing of 27 km and 3 nested domains with horizontal grid spacing of 9, 3 and 1 km, respectively. The inner-most domain is centred on the Pyramid station and covers an area of 288 km by 300 km. All nests have 61 vertical levels. The simulation is initialised with 0.5 degree Climate Forecast System Reanalysis (CFSR[37]) data. The surface topography data is from the United States Geological Survey (USGS) at a horizontal resolution of 30 arc seconds (1 km). During the simulation, the outer domain is nudged towards the reanalysis fields every 6 hours, but the nudging is only applied above the planetary boundary layer. Applying the nudging allows us to perform one continuous simulation, which is initialized at 00 UTC on 17 December 2014 and runs until 23:59 UTC on 21 December

2014. To ensure that the model did not become numerically unstable, we used an adaptive time step which was calculated based on a target Courant–Friedrichs–Lewy (CFL) criterion of 0.8. In addition, 6th order numerical diffusion was included and w-Rayleigh damping was applied over the upper-most 5 km of the model domain. Subgrid-scale physical processes were parameterized: microphysics by the Thompson scheme, long- and short-wave radiation by the RRTMG scheme. boundary-layer turbulence by the Mellor-Yamada-Janjic (Eta) TKE scheme and surface layer physics with the Monin-Obukhov similarity scheme.

FLEXPART simulations

FLEXPART (FLEXible PARTicle dispersion model[38]) is a Lagrangian particle dispersion model which calculates the trajectories of a large number of particles. Particles in FLEXPART do not necessarily directly represent real particles but rather can be thought to represent an infinitesimally small air parcel. Different versions of FLEXPART have been developed to work with meteorological input from a range of numerical weather and climate prediction models. In this study we use FLEXPART-WRF version 3.3.1[39].

For each day between 17 and 21 December 2014, a 24-hour simulation was conducted with output written every 30 minutes. In each simulation, two million particles were released within a layer 0 – 10 metres above ground level at a constant rate over a 6-hour period between 08:45 and 14:45 LT at the location of the Pyramid station The released particles are not affected by dry or wet deposition, radioactive decay nor any chemical processes and thus are passive tracers (and hereinafter referred to as such). The shallow release height mimics the observation height and makes it as hard as possible for the passive tracers to reach high altitudes.

Meteorological information and land use classification was read from the two inner most domain WRF output files every 10 minutes. Due to the high horizontal resolution of the input data, no

convection scheme was used in the FLEXPART simulations nor was any sub-grid terrain variability applied in the calculation of the planetary boundary layer height as recommended by reference 39. FLEXPART includes different options as to how the surface layer, planetary boundary layer depth and turbulence are represented. The mixed layer depth in FLEXPART is determined using a critical Richardson number method[40] and the minimum mixed layer depth is set to 100 m. While it is possible to read the turbulent kinetic energy direct from the WRF output and use this to represent turbulence, this is not recommended by reference 39 as this has been shown to violate the well-mixed criterion. Therefore, we use the FLEXPART internal turbulent scheme[41] to calculate turbulence and assume that in convective boundary layers the turbulence is Gaussian rather than skewed.

FLEXPART outputs (1) the position of each particle at each output time, (2) gridded output of particle concentrations in units of ng m^{-3} (c_{flex}), and (3) a highly condensed particle output, which includes the centroid position of all particles. The gridded particle concentration (ng m^{-3}) can be converted to the number of particles per unit volume (cm^{-3}). The particles transported in FLEXPART are assigned an arbitrary mass of $5 \cdot 10^{-4}$ kg (gravity has no impact on the particles). Hence, the number of FLEXPART particles per m^3 (N_{flex}) can be determined as:

$$N_{flex} = (C_{flex} \cdot 10^{-12}) / 5 \cdot 10^{-4}$$

Note that 1 ng = 10^{-12} kg. The number of released FLEXPART particles ($2 \cdot 10^6$) can then be scaled with the observed daily production of particles (N_{obs}) to estimate realistic particle number concentrations (N_{scaled}) :

$$N_{scaled} \ (m^{-3}) = N_{flex} \ (N_{obs} / 2 \cdot 10^6).$$

Estimation of the production of particles by NPF and their transportation to the free troposphere.

Daily particle production (DPP) has been estimated as the flux of particles with a diameter between 10 nm and 50 nm passing NCO-P during NPF events according to the equation below. DPP was computed for a NPF day assuming the valley to be "U"-shaped at NCO-P and having a width $L = 4$ km. The height of the flux cross-section was assumed to be a constant boundary layer height $h_{BL} = 300$ m. For each day, the particle flow was estimated as the product of the median of total particle count during the NPF event (N_{10-50}), the median wind speed (W_s) and the duration of the NPF event (t_{NPF}). The median DPP across all NPF events results in 2.1 10^{20} as seen from Fig. 5c.

$$\mathrm{DPP} = h_{BL} \mathrm{L}\, \mathrm{median}(N_{10\text{-}50})\, \mathrm{median}(W_s) t_{NPF}$$

Estimating the effect of particle venting by NPF

The number of released particles in the FLEXPART simulations was scaled with the actual number of vented particles (DPP=N_{obs}) to obtain effective particle concentrations in the troposphere. We calculated the air mass volume wherein particle concentrations exceeded 1 cm^{-3} and the corresponding average particle concentration in this volume. This is illustrated in Fig. 5b for 4 out of the 5 simulation days. On 17 December no NPF occurred. 9-12h after the start of NPF, particles are distributed in an air mass volume of 10000 – 30000 km^3 with average particle concentrations of 5-100 cm^{-3}. As shown in Extended Data Fig. 8, the majority of particles reside in the free troposphere. The particles are distributed over an area of roughly 30-50 x 80-150 km^2. The Duth Koshi basin has within 40 km about 3-5 valleys similar to the one, where the NCO-P station is located (Supplementary Fig. 17). We may expect that in all these valleys a similar wind regime

exists and NPF occurs. Thus, along a trajectory of 80 to 150 km an air mass may be fed by particles from 4-12 valleys. Therefore, we may expect concentrations of up to several hundred particles cm^{-3}. The background concentration of particles with $d < 50$ nm, estimated as the median concentration between 1:00 and 5:00 a.m., was around 450 cm^{-3}. Altogether, NPF and mountain venting of these small particles may increase the free tropospheric particle concentration above the Himalaya and downwind of it.

Data availability

Measurement and model output data for the analyses and figures in this study are archived at the Zenodo repository (https://doi.org/10.5281/zenodo.4022816). The WRF and FLEXPART model simulation results are stored on CSC – IT Centre for Science object oriented storage server Allas, and can be made available upon request from the corresponding author.

Code availability

The WRF model code is publically available, has a Digital Object Identifier (DOI) doi:10.5065/D6MK6B4K and can be obtained via github https://github.com/wrf-model/WRF. The FLEXPART-WRF model code is publically available and can be obtained from https://www.flexpart.eu/wiki/FpLimitedarea. The code for data processing is available upon request from the corresponding author.

References

26.   Marinoni, A. *et al.* High black carbon and ozone concentrations during pollution transport in the Himalayas: Five years of continuous observations at NCO-P global GAW station. *J. Environ. Sci.* **25**, 1618–1625 (2013).

27.	WMO *WMO/GAW Aerosol measurement procedures, guidelines and recommendations 2nd Edition*. (World Meteorological Organization: Geneva, Switzerland, 2016).

28.	Vanhanen, J. *et al.* Particle size magnifier for nano-CN detection. *Aerosol Sci. Tech.* **45**, 533–542 (2011).

29.	Kangasluoma, J. *et al.* Characterization of a Herrmann-type high-resolution differential mobility analyzer. *Aerosol Sci. Tech.* **50**, 222–229 (2016).

30.	Lehtipalo, K. *et al.* Methods for determining particle size distribution and growth rates between 1 and 3 nm using the Particle Size Magnifier. *Boreal Environ. Res.* **19**, 215–236 (2014).

31.	Rose, C. *et al.* Major contribution of neutral clusters to new particle formation at the interface between the boundary layer and the free troposphere. *Atmos. Chem. Phys.* **15**, 3413–3428 (2015).

32.	Manninen, H. E., Mirme, S., Mirme, A., Petäjä, T. & Kulmala, M. How to reliably detect molecular clusters and nucleation mode particles with Neutral cluster and Air Ion Spectrometer (NAIS). *Atmos. Meas. Tech.* **9**, 3577–3605 (2016).

33.	Mirme, S. & Mirme, A. The mathematical principles and design of the NAIS – a spectrometer for the measurement of cluster ion and nanometer aerosol size distributions. *Atmos. Meas. Tech.* **6**, 1061–1071 (2013).

34.	Wagner, R. *et al.* On the accuracy of ion measurements using a Neutral cluster and Air Ion Spectrometer. *Boreal Environ. Res.* **21**, 230–241 (2016).

35.	Junninen, H. *et al.* A high-resolution mass spectrometer to measure atmospheric ion composition. *Atmos. Meas. Tech.* **3**, 1039–1053 (2010).

36.	Jokinen, T. *et al.* Atmospheric sulphuric acid and neutral cluster measurements using CI-APi-TOF. *Atmos. Chem. Phys.* **12**, 4117–4125 (2012).

37.	Saha, S. *et al.* The NCEP climate forecast system reanalysis. *Bull. Amer. Meteor. Soc.* **91**, 1015–1058 (2010).

38.   Stohl, A., Forster, C., Frank, A., Seibert, P. & Wotawa, G. Technical note: The Lagrangian particle dispersion model FLEXPART version 6.2. *Atmos. Chem. Phys.* **5**, 2461–2474 (2005).

39.   Brioude, J. *et al.* The Lagrangian particle dispersion model FLEXPART-WRF version 3.1. *Geosci. Model Dev.* **6**, 1889–1904 (2013).

40.   Vogelezang, D. H. P. & Holtslag, A. A. M. Evaluation and model impacts of alternative boundary-layer height formulations. *Boundary Layer Meteor.* **81**, 245–269 (1996).

41.   Hanna, S. R. *Atmospheric turbulence and air pollution modelling Ch.7* . (D. Reidel Publishing Company, Dordrecht/Boston/Lancaster, 1982).